*J. Fluid Mech.* (1992), *vol.* 237, *pp.* 479–498
*Printed in Great Britain*



# Controlling chaos in a thermal convection loop

By YUZHOU WANG, JONATHAN SINGER AND HAIM H. BAU†

Department of Mechanical Engineering and Applied Mechanics, University of Pennsylvania, Philadelphia, PA 19104–6315, USA

(Received 24 May 1991)

It is demonstrated experimentally and theoretically that through the use of an active (feedback) controller one can dramatically modify the nature of the flow in a toroidal thermal convection loop heated from below and cooled from above. In particular, we show how a simple control strategy can be used to suppress (laminarize) the naturally occurring chaotic motion or induce chaos in otherwise time-independent flow. The control strategy consists of sensing the deviation of fluid temperatures from desired values at a number of locations inside the loop and then altering the wall heating to either counteract or enhance such deviations.

## 1. Introduction

Chaotic behaviour is abundant both in nature and in manmade devices. On occasion, chaos is a desired feature as it enhances mixing and chemical reactions and provides a vigorous mechanism for transporting heat and/or mass. However, in many other situations, chaos is an undesired phenomenon which may lead to vibrations, irregular operation, fatigue failure in mechanical systems, temperature oscillations which may exceed safe operational conditions in thermal systems, and increased drag in flow systems. Also, since chaotic behaviour cannot be predicted in detail, it may be detrimental to the smooth operation of various devices. Clearly, the ability to control chaos (i.e. promote or eliminate it) is of much practical importance.

To date, most of the work in this area has focused on using predetermined means (in contrast to feedback control) to control the nature of flows. For example, Ottino (1989) used modulated (furrowed) conduits to promote chaos and enhance mixing and Wang & Bau (1990, 1991) demonstrated that time-periodic heating in a thermal convection loop might advance the transition to chaos. Much less attention has been given to the possibility of modifying the nature of convective flows through the use of feedback control which exploits or suppresses naturally occurring instabilities in the flow.

We believe that feedback control strategies hold considerable promise as a practical means of modifying flows so as to achieve a desired behaviour. Recently, Ott, Grebogi & Yorke (1990*a*, *b*) argued and demonstrated through numerical experiments with the Henon map that one can stabilize the otherwise chaotic motion about any pre-chosen non-stable orbit through the use of relatively small perturbations. Their ideas were put into practice by Ditto, Rauseo & Spano (1990) who succeeded in stabilizing some of the periodic orbits within the chaotic attractor of a vibrating magnetostrictive ribbon whose Young modulus varied as a function of the imposed magnetic field. In Singer, Wang & Bau (1991), we demonstrated experimentally that through the use of feedback control, one can maintain stable

† All correspondence should be directed to this author.

steady flow in a thermal convection loop with heating conditions that in the absence of a controller would lead to chaotic flow. The present paper is an extension of and elaboration on Singer *et al.* 1991.

In this paper, we investigate experimentally and theoretically a relatively simple convective system – the thermal convection loop. This system was chosen for investigation because it exhibits a rich collection of flow structures ranging from no motion to steady motion to chaos and yet it can be analysed, at least qualitatively, using a low-dimensional dynamic model. Moreover, even though this system is a relatively simple one, it is, nonetheless, important since thermal convection loops provide a means for circulating fluid without the use of pumps. Such loops are of interest for solar heaters, emergency reactor-core cooling, and process industries. They also are of interest for understanding warm springs, seawater circulation in the oceanic crust, and formation of ore deposits. For a general review of the applications and an analysis of these loops, see the article by Metrol & Greif (1985) and the literature cited therein.

## 2. Theoretical study

In this section, we set forth a simple mathematical model for the flow in the loop, summarize briefly the solutions of the governing equations for the uncontrolled system and then modify these equations to include a feedback controller. Finally, we analyse the controlled system.

### 2.1. *The governing equations*

Consider a thermal convection loop constructed from a pipe bent into a torus and standing in the vertical plane as depicted in figure 1. The diameter of the pipe is $d$; and the diameter of the torus is $D$. $\theta$ is the angular location of a point on the torus. The wall temperature of the pipe $T_w(\theta, t)$, which may vary both with the angular location $\theta$ and the time $t$, is symmetric with respect to the torus axis that is parallel to the gravity vector. Variations in the wall temperature may cause a spatial temperature distribution inside the fluid which, under appropriate conditions, may induce fluid motion in the loop.

We analyse the motion in the loop within the framework of Boussinesq's approximation using a one-dimensional model consisting of mass, momentum and energy balances (Bau & Torrance 1981):

$$u = u(t), \tag{1}$$

$$\dot{u} = \frac{1}{\pi} Ra\, P \oint T \cos(\theta)\, \mathrm{d}\theta - Pu, \tag{2}$$

and

$$\dot{T} = -u\frac{\partial T}{\partial \theta} + B\frac{\partial^2 T}{\partial \theta^2} + [T_w(\theta, t) - T]. \tag{3}$$

The fluid is assumed to be incompressible and Newtonian. In the above, all quantities are non-dimensional; $Ra = g\beta\Delta T\tau^2/(DP)$ is the loop's Rayleigh number; $\beta$ is the thermal expansion coefficient; $g$ is the gravitational acceleration; and $\Delta T$ is the averaged wall temperature difference between the loop's bottom and top. The timescale is $\tau = \rho_0 C_p d/(4h)$, where $\rho_0$ is the fluid's average density, $C_p$ is the thermal capacity, and $h$ (which we assume to be constant) is the heat transfer coefficient between the fluid and the pipe's wall. $P = 32\nu\tau/d^2 = 8Pr/Nu$ is the loop's Prandtl number, where $\nu$ is the kinematic viscosity. $Pr = \nu/\alpha$ and $Nu = hd/k$ are the

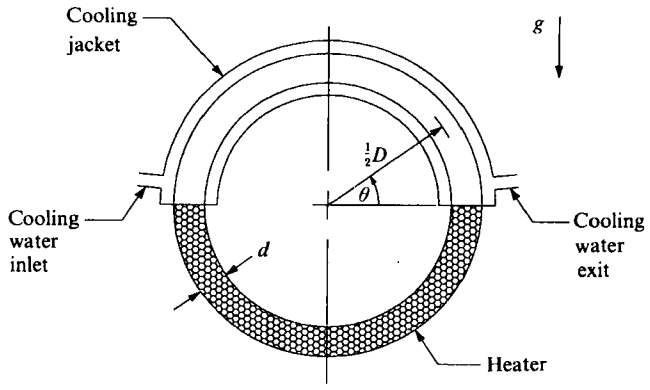


FIGURE 1. Schematic description of the experimental apparatus.

conventional Prandtl and Nusselt numbers, respectively. $\alpha$ and $k$ are the fluid's thermal diffusivity and conductivity; and $B = (d/D)^2/Nu$ is the Biot number. The lengthscale is the torus radius, $\frac{1}{2}D$.

In addition to the aforementioned Boussinesq's approximation, the mathematical model presented here assumes implicitly that the friction and heat transfer laws are similar to those of laminar, fully developed, Poiseuille pipe flow. One would expect, and we did in fact observe in the experiments, the development of secondary circulation which may significantly modify both the friction and heat transfer laws (but which has the positive effect of improving temperature uniformity at each cross-section of the loop). Unfortunately, more realistic friction and heat transfer laws are not known *a priori*. To obtain these correlations, one may need to solve a spatially three-dimensional model or conduct experiments. We justify the use of the simpler correlations above on the grounds that the model still provides a qualitatively correct picture as has been confirmed by our own experiments (§3.2 below) and those by others (i.e. Ehrhard & Muller 1990; Gorman, Widmann & Robins 1984, 1986; Widmann, Gorman & Robins 1989) as well as by theoretical studies by Hart (1984, 1985) and Yorke, Yorke & Mallet-Paret (1987) in which more complicated heat transfer and friction factor correlations were used.

Next, we expand the wall and fluid temperatures in Fourier series in terms of the angle $\theta$:

$$T_w(\theta, t) = W_0(t) + \sum_{n=1}^{\infty} W_n(t) \sin(n\theta), \tag{4}$$

and

$$T(\theta, t) = \sum_{n=0}^{\infty} S_n(t) \sin(n\theta) + C_n(t) \cos(n\theta). \tag{5}$$

Upon substituting the series (4), (5) into the governing equations (1)–(3) and requiring that these equations be satisfied in the sense of weighted residuals, we obtain an infinite set of ordinary differential equations. Three equations which are similar to the celebrated Lorenz (1963) equation, decouple from the rest of the set (with exact closure) and can be solved independently of the other equations without need of truncation (Malkus 1972). Thus, one can obtain a description of the dynamics of the flow by solving these three equations:

$$\dot{u}/P = c - u, \tag{6}$$

$$\dot{c} = -us - c \tag{7}$$

$$\dot{s} = uc - s + RaW_1. \tag{8}$$

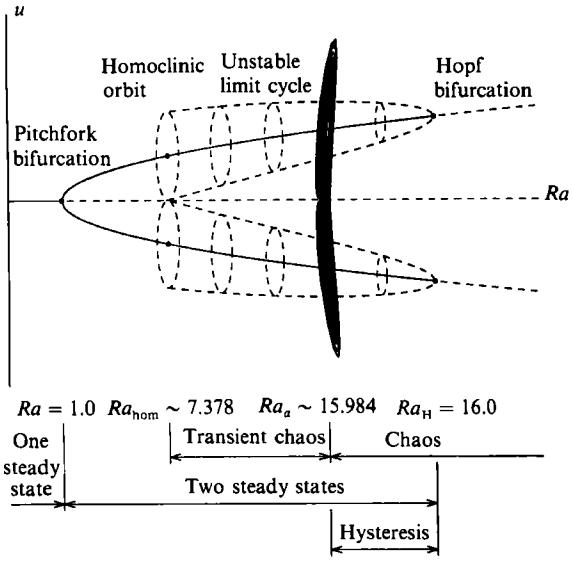


FIGURE 2. An unscaled bifurcation diagram depicting various possible solutions as the Rayleigh number is increased ($P = 4$). Stable and non-stable solutions are denoted by solid and dashed lines, respectively. The dark region represents the appearance of the strange attractor which exists for $Ra > Ra_a$.

In the above, we removed the dependence on the Biot number, $B$, via the simple, algebraic transformation $\{u, c, s, Ra, P, t\} \leftarrow 1/(1+B)\ \{u, Ra\,C_1, Ra\,S_1, Ra/(1+B), P, t(1+B)^2\}$. Roughly speaking, the quantities $c$ and $s$ are proportional, respectively, to the temperature differences in the fluid between the 3 and 9 o'clock and 6 and 12 o'clock positions around the loop.

### 2.2. *The uncontrolled flow – a summary*

The set (6)–(8) with $W_1 = -1$ are the celebrated Lorenz (1963) equations and have been investigated exhaustively in the literature (for reviews, see for example, Sparrow 1982 and Bau & Wang 1991). Here, we summarize very briefly some details relevant to the present study. The equations (6)–(8) with $W_1 = -1$ possess a number of non-transient solutions, such as: (*a*) no-motion state ($u = c = 0$, $s = -Ra$); (*b*) time-independent motion either in the clockwise (denoted $B_-$) or counterclockwise (denoted $B_+$) direction ($u = c = \pm(Ra-1)^{\frac{1}{2}}$, $s = -1$); (*c*) chaotic motion; (*d*) periodic motions of various periodicities.

Some of the above solutions and their stability characteristics are depicted schematically in figure 2 for a loop Prandtl number $P = 4$ which we estimate to approximate the loop Prandtl number of our experimental apparatus (Singer 1991). In figure 2, we denote stable and non-stable solutions by solid and dashed lines, respectively. Briefly, if one were to follow the chain of events as the Rayleigh number ($Ra$) increases, one would observe no net motion in the loop for $Ra < 1$. At $Ra = 1$, the no-motion solution loses its stability through a supercritical pitchfork bifurcation and is replaced by a time-independent motion. Depending on random disturbances, this motion will be either in the clockwise ($B_-$) or counterclockwise ($B_+$) direction. The motion solution is stable for $1 < Ra < Ra_H(P) = P(P+4)/(P-2)$, where $Ra_H(4) = 16$. At that point the steady solution loses stability through a subcritical Hopf bifurcation. The resulting limit cycle (equation (11) below with $K = 0$) is non-

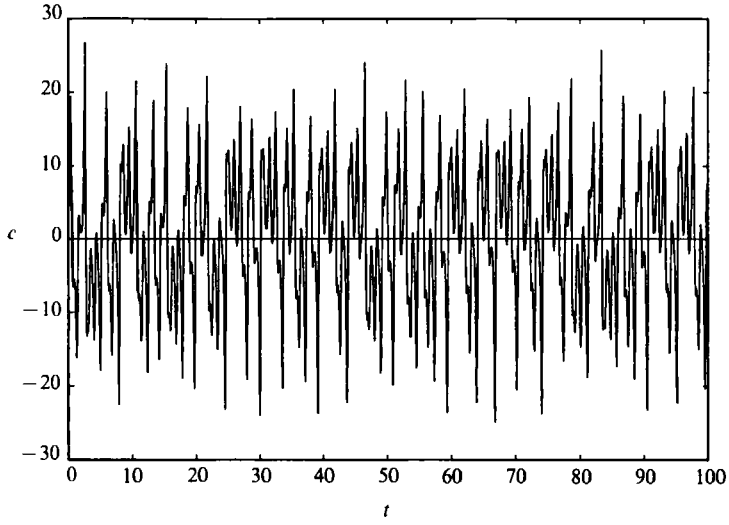


FIGURE 3. The temperature difference between the 3 and 9 o'clock positions is depicted as a function of time for $Ra \sim 3Ra_{\mathrm{H}} = 48$.

stable and its period increases to infinity as the Rayleigh number decreases to $Ra_{\mathrm{hom}}(P)$. At $Ra_{\mathrm{hom}}(4) \sim 7.378$, the periodic orbit becomes an homoclinic orbit and passes through the no-motion state ($a$). At $Ra = Ra_{\mathrm{hom}}(P)$, there is a bifurcation (the homoclinic explosion) which results in an assortment of non-stable periodic and non-periodic orbits, known collectively as the non-wandering set, which is initially non-attracting. As the Rayleigh number is further increased beyond $Ra_a(P) \leqslant Ra_{\mathrm{H}}(P)$, where $Ra_a(4) \sim 15.984$, the non-wandering set becomes a strange (the Lorenz) attractor. The chaotic regime exists for $Ra > Ra_a$ with occasional windows of periodic behaviour. In the chaotic regime, the motion in the loop consists of irregular oscillations with occasional reversals in the direction of the flow as shown, for example, in figure 3 for $P = 4$ and $Ra = 3Ra_{\mathrm{H}}(4) = 48$. In figure 3, we depict the temperature difference ($c$) between positions 3 and 9 o'clock as a function of time. The positive and negative values of $c$ in figure 3 correspond to flow in the counterclockwise and clockwise directions, respectively. In §3.2, we show that qualitatively similar behaviour is observed in our experiments.

### 2.3. *Active control of the flow*

In this section, we focus on the stabilization and destabilization of the time-dependent motion solution ($B_+$). That is, we wish to obtain (i) steady, non-oscillatory flow under conditions in which the uncontrolled flow is nominally chaotic ($Ra > Ra_{\mathrm{H}}$) without significantly changing the operating conditions and structure of the loop; and (ii) chaotic flow under conditions for which the uncontrolled flow is nominally time-independent ($Ra < Ra_{\mathrm{H}}$). In our experiments, we used the temperature difference, $c(t)$, between the 3 and 9 o'clock positions around the loop as the controlling signal and the power input to the heater as the controlled signal. In the mathematical model, we control the wall temperature which is proportional to the power input.

The time-dependent solution at $Ra$ is $c(t) = \bar{c} = (Ra-1)^{\frac{1}{2}}$. For $Ra > Ra_{\mathrm{H}}$, this solution is nominally non-stable and $c(t)$ varies as a function of time in a rather complicated way (see figure 3 for an example). We wish to modify the wall

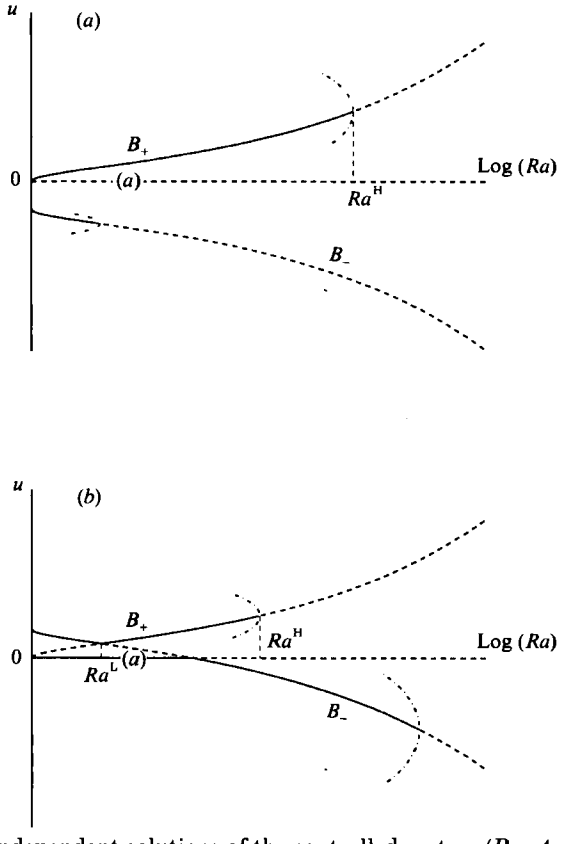


FIGURE 4. The time-independent solutions of the controlled system ($P = 4$ and $K$ is fixed). $K = -2$ and 2 in ($a$) and ($b$), respectively. The solid and dashed lines correspond, respectively, to linearly stable and non-stable solutions.

temperature so as to retain $c(t) = \bar{c}$. To this end, we change the wall temperature in proportion to the deviation of $c(t)$ from the desired value $\bar{c}$ as

$$W_1 = -1 - \frac{K}{Ra}(c(t) - \bar{c}), \tag{9}$$

where $K$ is the controller's gain. Note that (6)–(9) are invariant under the transformation $\{u, c, s, \bar{c}, K\} \rightarrow \{-u, -c, s, -\bar{c}, -K\}$. Thus, we may except that values of $K$ which stabilize the counterclockwise motion ($B_+$) will destabilize the clockwise motion ($B_-$) and vice versa.

Next, we calculate the time-independent solutions of the augmented system (6)–(9) and establish their stability characteristics. These solutions are depicted as functions of the Rayleigh number in figures 4($a$) ($K = -2$) and 4($b$) ($K = 2$) for negative and positive gains and for $P = 4$. The solid and dashed lines in figure 4 correspond, respectively, to linearly stable and non-stable solutions. Here, of prime interest to us, is the counterclockwise-motion solution $\{B_+ : u = c = (Ra-1)^{\frac{1}{2}},\ s = 1\}$ which is the same for both the uncontrolled and controlled systems and whose stability characteristics we wish to alter. The clockwise-motion solution of the controlled system is $\{B_- : u = c = K-(Ra-1)^{\frac{1}{2}},\ s = -1\}$. The controlled system also admits the no-motion solution $\{a : u = c = 0,\ s = -Ra+K(Ra-1)^{\frac{1}{2}}\}$.

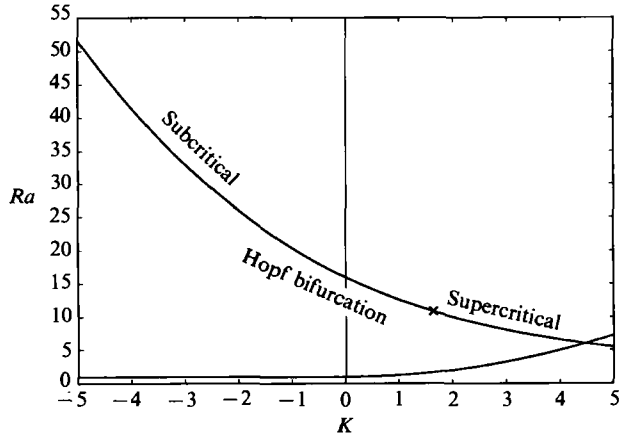


FIGURE 5. Stability characteristics of the counterclockwise-motion solution under proportional control. The critical Rayleigh number is depicted as a function of the controller's gain ($K$).

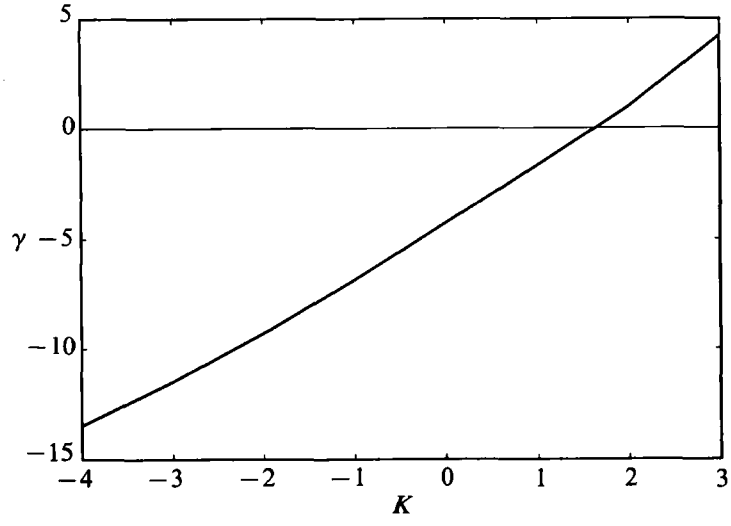


FIGURE 6. The amplitude of the limit cycle, $\gamma(P,K)$, is depicted for $P = 4$ as a function of $K$. Positive (negative) values of $\gamma(P,K)$ correspond to super (sub) critical bifurcation.

### 2.3.1. *The counterclockwise motion solution and its stability under active control*

Linear stability analysis of (6)–(9) conducted for small disturbances around the time-independent flow ($B_+$) leads to the following characteristic equation for the growth rate $\sigma$:

$$\sigma^3+(P+2)\,\sigma^2+[Ra+P-K(Ra-1)^{\frac{1}{2}}]\,\sigma+P(Ra-1)^{\frac{1}{2}}\,(2(Ra-1)^{\frac{1}{2}}-K)=0. \quad (10)$$

This equation suggests that the counterclockwise solution ($B_+$) is stable for $Ra$ values which satisfy

$$2(Ra-1)^{\frac{1}{2}} \geqslant K \quad \text{and} \quad \frac{(P-2)\,[Ra-Ra_{\mathrm{H}}(P)]}{2(Ra-1)^{\frac{1}{2}}} \leqslant -K.$$

We denote the $Ra$ values at the low and high marginal stability limits as $Ra^{\mathrm{L}}(K)$ and $Ra^{\mathrm{H}}(P,K)$, respectively. The magnitude of the low (high) stability limits is independent of (dependent on) the loop's Prandtl number ($P$). In figure 5, both stability limits are depicted as functions of the gain $K$ for $P = 4$.

It is apparent from figure 5 that negative (positive) values of $K$ serve to stabilize

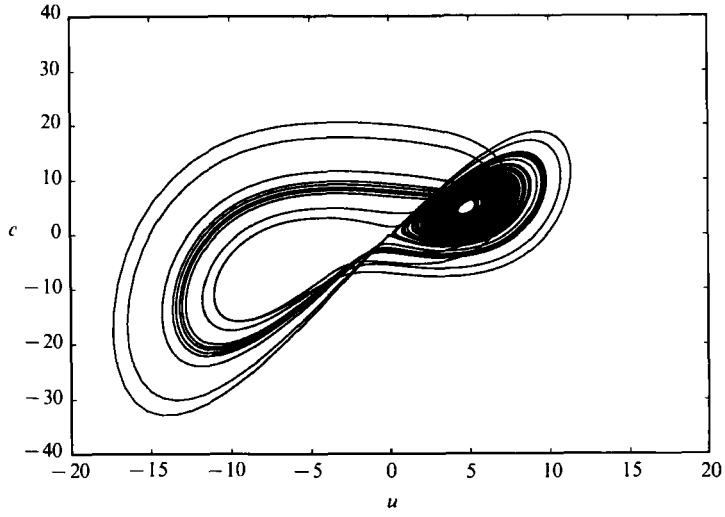


FIGURE 7. The '$uc$' projection of the motion trajectories for the controlled system with $Ra$ exceeding the marginal stability limit ($K = -2$, $P = 4$, and $Ra = 50$).

(destabilize) the counterclockwise-motion solution. The low limit of stability, $Ra^{\mathrm{L}}(K)$, corresponds to a bifurcation through a simple eigenvalue (exchange of stability). Along the line $Ra^{\mathrm{L}}(K)$, the counterclockwise-motion solution ($B_+$) intersects at $Ra^{\mathrm{L}}(K) = 1$ with the no-motion solution for $K < 0$ (figure 4$a$) and at $Ra^{\mathrm{L}}(K) = 1 + \frac{1}{4}K^2$ with what eventually will become the clockwise-motion solution ($B_-$) for $K > 0$ (figure 4$b$).

The upper stability limit

$$Ra^{\mathrm{H}}(P,K) = 1 + \left(\frac{[(P^2-4)(P+1)+K^2]^{\frac{1}{2}}-K}{P-2}\right)^2$$

corresponds to a Hopf bifurcation which gives birth to a limit cycle. We used the 'projection technique' described in Iooss & Joseph (1989) to calculate the limit cycle. Since the procedure is somewhat lengthy we do not provide the derivation here. The interested reader is referred to Wang's (1991) dissertation for details. In the vicinity of the bifurcation point, the limit cycle can be described, to a first approximation, by

$$\begin{pmatrix} u \\ c \\ s \end{pmatrix} = \begin{pmatrix} (Ra^{\mathrm{H}}(P,K)-1)^{\frac{1}{2}} \\ (Ra^{\mathrm{H}}(P,K)-1)^{\frac{1}{2}} \\ -1 \end{pmatrix} + 2\left[\frac{Ra-Ra^{\mathrm{H}}(P,K)}{\gamma(P,K)}\right]^{\frac{1}{2}} \begin{bmatrix} \cos[(\omega(P,K)t] \\ \cos[\omega(P,K)t]-(\omega_0/P)\sin[(\omega(P,K)t)] \\ A_1\cos[\omega(P,K)t]-A_2\sin[(\omega(P,K)t] \end{bmatrix}, \tag{11}$$

where $\gamma(P,K)$ is depicted in figure 6 as a function of $K$ for $P = 4$. In the above,

$$\omega^2(P,K) \sim \omega_0^2 = Ra^{\mathrm{H}} + P - K(Ra^{\mathrm{H}}-1)^{\frac{1}{2}}, \quad A_1 = \frac{(\omega_0^2+2P)(Ra^{\mathrm{H}}-1)^{\frac{1}{2}}-K\omega_0^2-KP}{P(\omega_0^2+1)},$$

$$A_2 = -\omega_0 \frac{(2P-1)(Ra^{\mathrm{H}}-1)^{\frac{1}{2}}+K(1-P)}{P(\omega_0^2+1)}.$$

Positive and negative values of $\gamma(P,K)$ correspond, respectively, to super- and subcritical bifurcations. For $K < K_0 \sim 1.635$, the resulting limit cycle is subcritical while for $2(1+P)^{\frac{1}{2}} > K > K_0$, it is supercritical. As the loss of stability of $B_+$ is strict ($Re\,(\partial\sigma/\partial Ra > 0$ for all $K$), supercritical (subcritical) limit cycles are (non) stable.

For $Ra < Ra^{H}(P,K)$, the counterclockwise motion ($B_+$) is stable with respect to small disturbances. For $Ra > Ra^{H}(P,K)$ this solution loses stability. Depending on the value of $K$, one may observe various types of behaviour. For $K < 0$, the system will exhibit oscillatory, chaotic behaviour with occasional reversals in the flow direction. The trajectories in phase space will tend, however to spend more time around $B_+$ than $B_-$. That is, most of the time the flow will be in the counterclockwise direction. See, for example, figure 7, where we depict the '*uc*' projection of the chaotic motion trajectories for $K = -2$, $P = 4$, and $Ra > Ra^{H}$.

For $0 < K < K_0$, after initial, chaotic transients die out, the system will tend to stabilize at $B_-$. For $K_0 < K < 2(P+1)^{\frac{1}{2}}$, the limit cycle generated at the Hopf bifurcation is stable. Thus, depending on initial conditions, one may observe either periodic oscillations around $B_+$ or a stable clockwise motion ($B_-$). Suppose we have time-independent counterclockwise motion ($B_+$) in the loop corresponding to $Ra = 9$ and $K = 2$. That is, we are within the stable region of figure 5. Now we gradually increase the Rayleigh number but maintain the controller's gain fixed at $K = 2$. This corresponds to moving along the vertical line $K = 2$ in figure 5. The chain of events is described in figure 8 where the velocity $u$ is depicted as a function of the Rayleigh number. The $u$-values shown in figure 8 correspond to the intersection of the phase-space trajectories with the Poincaré plane $s = -1$. For $Ra < 10$, we observe stable $B_+$ motion. At $Ra = 10$, this solution undergoes a supercritical Hopf bifurcation into a stable limit cycle, a sample of which we depict in figure 9 for $Ra = 10.5$. The period of the limit cycle increases gradually as the Rayleigh number increases. At $Ra \sim 10.6$, the limit cycle loses stability. After transients die out (not shown in figure 8), the system settles down into a clockwise motion state ($B_-$).

The lower and upper limits of stability intersect at $K = 2(1+P)^{\frac{1}{2}}$ in figure 5. At this point, the bifurcation occurs through a double eigenvalue. For larger values of $K$, no stable, steady, counterclockwise-motion solutions exist. In numerical experiments, we have observed in this region a variety of periodic orbits; but, as the region of $K > 2(1+\mathrm{P})^{\frac{1}{2}}$ is not central to this paper, we do not report any further results here.

### 2.3.2. *The clockwise-motion solution ($B_-$) and its stability*

The controller changes the nature of the clockwise solution from that of the uncontrolled system. The stability characteristics of this solution ($B_-$) are depicted for $K < 0$ and $K > 0$ in figures 4(*a*) and 4(*b*), respectively. For $K < 0$ (figure 4*a*), this solution is stable for $1 < Ra < m^2+1$, where

$$m = \frac{[(P^2-4)(P+1)+K^2]^{\frac{1}{2}}+K(P-1)}{P-2}.$$

The upper boundary of stability corresponds to a Hopf bifurcation. For $K > 0$ and $Ra < K^2+1$, the $B_-$ solution corresponds to flow in the counterclockwise direction. At $Ra = 1+\frac{1}{4}K^2$, the solutions $B_-$ and $B_+$ intersect (figure 4*b*). The counterclockwise motion part of $B_-$ is linearly stable for $1 < Ra < 1+\frac{1}{2}K^2$ and $K < 2(1+P)^{\frac{1}{2}}$. That is, a stable no-motion solution and a counterclockwise-motion solution coexist in this interval.

### 2.3.3. *The no-motion solution and its stability*

The controller does not affect the stability characteristics of the no-motion solution. For $K < 0$, the no-motion solution is stable for $Ra < 1$. For $K > 0$, this solution is stable for $Ra < 1+K^2$. This, however, does not represent stabilization of the no-motion state as the effective Rayleigh number corresponding to the

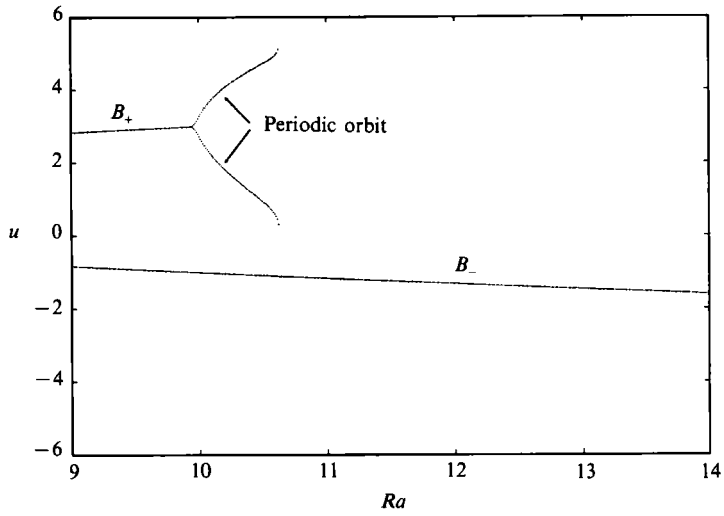


FIGURE 8. The velocity $u$ is depicted as a function of the Rayleigh number $Ra$. The $u$-values shown correspond to the intersection of the phase-space trajectories with the plane $s = -1$.

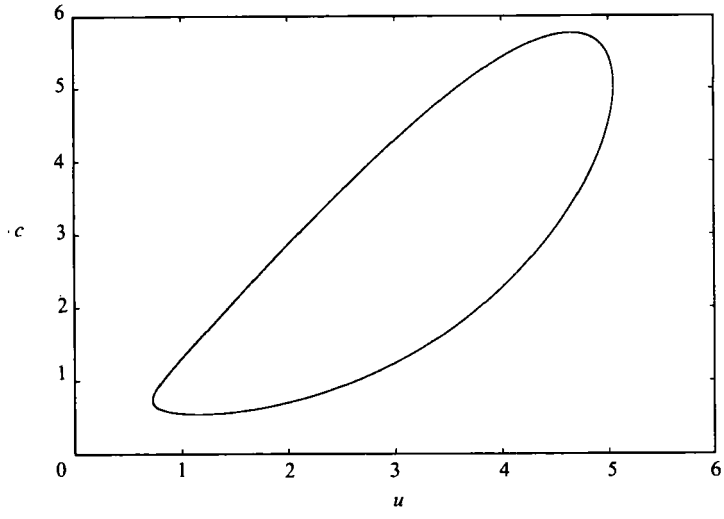


FIGURE 9. The orbit of a limit cycle generated through supercritical Hopf bifurcation for $Ra = 10.5$, $P = 4$, $K = 2$.

aforementioned stability limit $Ra_{\text{eff}} = Ra - K(Ra = 1)^{\frac{1}{2}} = 1$. In order to stabilize the no-motion state, one needs to employ a different control strategy than the one described here (i.e. that of Singer & Bau 1991).

### 2.3.4. *The effect of the controller on the flow*

In order to examine the impact of the controller on the dynamics of the flow, we conducted a few numerical experiments. In figure 10, we depict the temperature difference between the 3 and 9 o'clock positions ($c$) as a function of time for the controlled ($K = -35$, solid line) and uncontrolled ($K = 0$, dotted line) systems for $Ra = 50$ and $P = 4$. This is 3.125 times the critical value of the Rayleigh number needed to induce chaos in the uncontrolled system. The uncontrolled signal exhibits oscillatory, chaotic behaviour with occasional reversals in the direction of the flow while the controlled signal, after the initial oscillations die out, corresponds to a time-

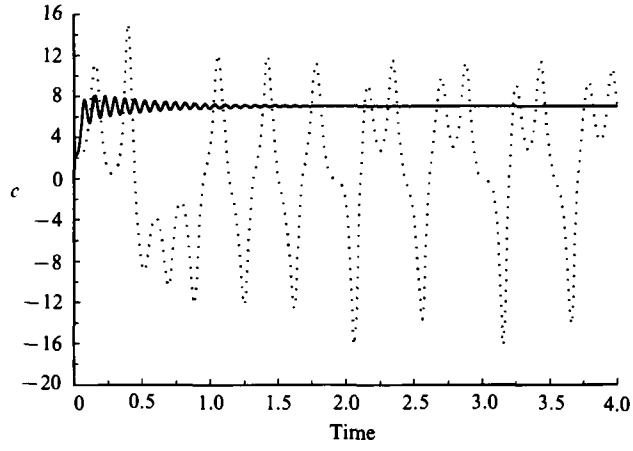


FIGURE 10. The temperature difference between the 3 and 9 o'clock positions is depicted for $Ra = 50$ and $P = 4$ as a function of time for the controlled ($K = -35$, solid line) and the uncontrolled ($K = 0$, dotted line) systems.

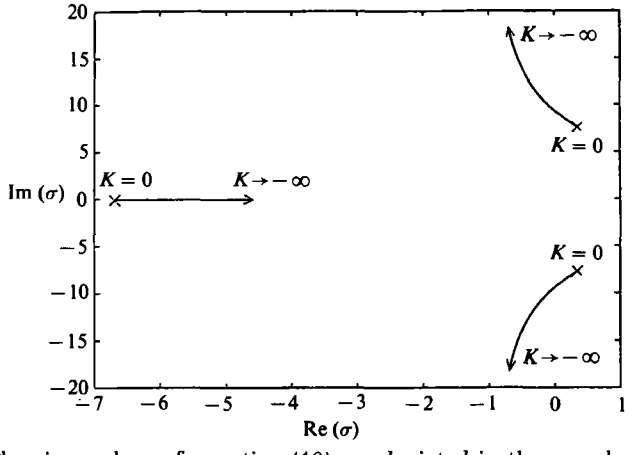


FIGURE 11. The eigenvalues of equation (10) are depicted in the complex plane as functions of the controller's gain for $K < 0$, $Ra = 50$ and $P = 4$.

independent flow. The controller is capable of restoring the counterclockwise flow to its steady-state value in the presence of finite-amplitude disturbances as long as these disturbances remain within the domain of attraction of the controlled solution.

To understand the effect of the controller's gain on the system's stability, we depict in figure 11 the location of the eigenvalues ($\sigma$) of equation (10) in the complex plane as a function of the gain ($K$) for $Ra = 50$. For $K = 0$, there are two complex-conjugate eigenvalues with a positive real part (for $Ra = 50$, the uncontrolled system is non-stable). As $K$ decreases below zero, the real part of the complex-conjugate pair decreases until it crosses the imaginary axis at the marginal stability limit ($K = -4.857$). A further decrease leads to stabilization of the counterclockwise-motion solution. The real part of the eigenvalue (figure 11) dictates the rate of approach of $c(t)$ to its steady, time-independent value ($\bar{c}$). The imaginary part is responsible for the oscillatory transient depicted in figure 10. As the ratio $Re(\sigma)/\mathrm{Im}(\sigma)$ is relatively small, the transient is relatively long. Note that in the absence of noise, the controlled system operates with virtually the same power input as the uncontrolled one, but with a vastly different flow structure.

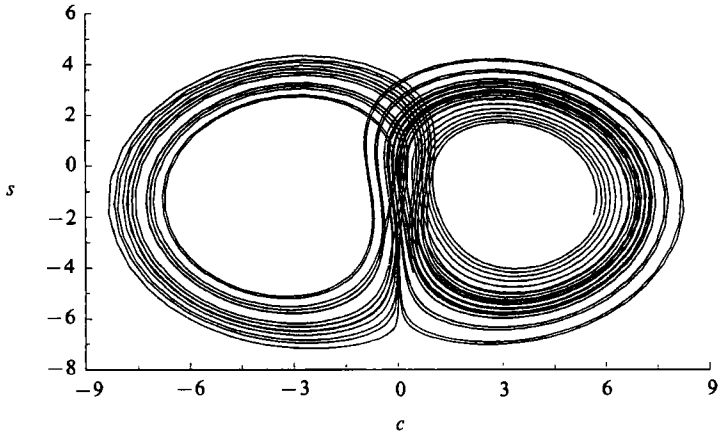


FIGURE 12. Destabilization of stable solutions. The '$cs$' projection of the attractor's phase portrait for $Ra = 13$, $K = 1$, and $P = 4$.

The analysis above suggests that positive values of $K$ destabilize the counter-clockwise motion ($B_+$). Since the same values of $K$ stabilize the clockwise motion ($B_-$), use of a controller with a positive gain ($K > 0$) will result in reversing the direction of the flow. If we wish to obtain oscillatory, chaotic flow for heating rates smaller than those at which such flow would normally occur in the uncontrolled system, we need to destabilize both solution branches, $B_+$ and $B_-$, simultaneously. This can be accomplished by modifying the controller to yield

$$W_1 = -1 - \frac{K}{Ra}[\mathrm{sgn}\,(c)\,c(t) - \bar{c}].$$

The results of this strategy are depicted in figure 12 for $Ra = 13 < Ra^{\mathrm{H}}$, $K = 1$, and $P = 4$. In this figure, we show the '$cs$' projection of a phase portrait of the attractor. The corresponding time series for $c$ (not shown) is qualitatively similar to the one depicted in figure 3. In the case of destabilization, the effective Rayleigh number of the loop will vary widely as a function of $c(t)$.

## 3. Experiments

In this section, we first describe the experimental apparatus, then we demonstrate that the flow observed in the loop is qualitatively similar to the predicted one, and finally, we show that the control strategy described in §2.3 can actually be used in practice.

### 3.1. *Description of the experimental apparatus*

The experimental apparatus is similar to that employed by Creveling *et al.* (1975), Gorman *et al.* (1984, 1986), and Widmann *et al.* (1989). The apparatus (figure 1) consists of a Pyrex pipe of diameter $d$ ($= 0.030$ m) bent into a torus of diameter $D$ ($= 0.760$ m). The apparatus stands in the vertical plane. The lower half of the apparatus is heated with a uniform-heat-flux resistance heater while the upper half is submerged in a jacket containing a flowing coolant. The coolant is circulated at a sufficiently high flow rate to approximate a uniform wall temperature. The heater consists of a metallic layer (instatherm) coated directly on the glass tube. This arrangement assures low thermal resistance between the glass tube and the heater. The heater is well insulated to minimize heat losses to the ambient. The power supply to the heater is computer controlled.

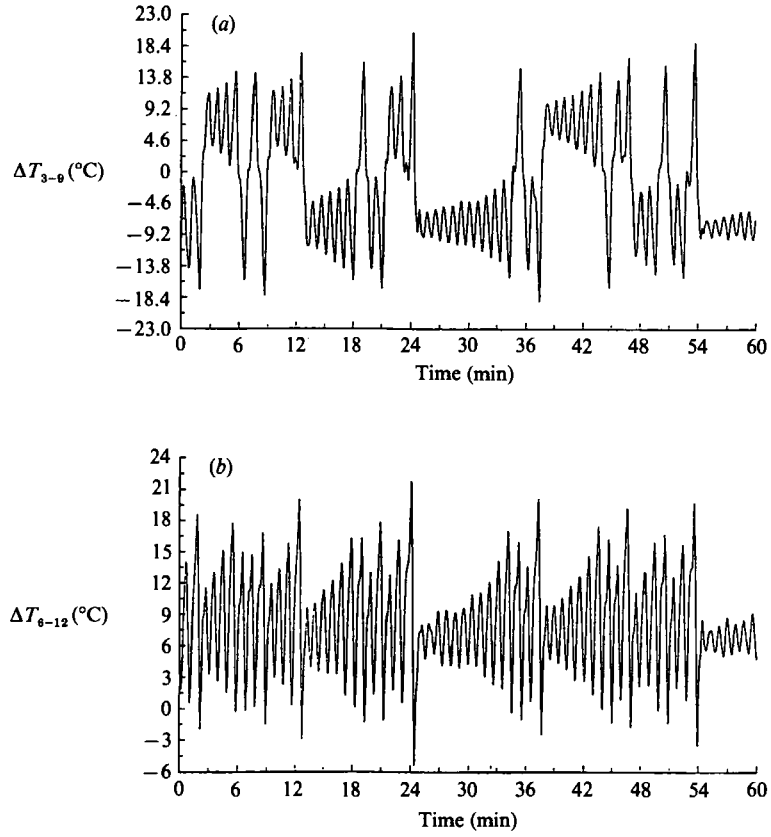


FIGURE 13. The experimentally measured temperature differences, (*a*) $\Delta T_{3-9}$ and (*b*) $\Delta T_{6-12}$, are depicted as functions of time for a heating input of 700 W. The system is not controlled.

In our experiments, we measured the power input to the heaters, the coolant's temperature and the temperature differences between the 3 and 9 o'clock positions and between the 6 and 12 o'clock positions around the loop which we denote as $\Delta T_{3-9}$ and $\Delta T_{6-12}$, respectively. All quantities were continuously monitored as functions of time with the aid of a computer-controlled data acquisition system. The direction of the flow in the loop, and to some extent, the velocity profile could be directly observed owing to the presence of small particles in the liquid.

### 3.2. *The uncontrolled flow in the loop*

Below, we briefly describe the various flow regimes observed in the loop as a function of the input heating rate in the absence of a controller. When heating and cooling were applied to an isothermal loop, depending on (stochastic) initial conditions and the loop's imperfections, the fluid motion occurred either in the counterclockwise or the clockwise direction. For relatively low heating rates, the flow inside the loop was time-independent and unidirectional. As the heating rate exceeded some critical value ($Q_c$), the flow became oscillatory and time-dependent with occasional reversals in direction. The critical heating rate $Q_c$ depended on the coolant's temperature. For example, for coolant temperatures of 8 and 20 °C, $Q_c \sim 315$ and 215 W, respectively.

Representative experimental results for the time-dependent flow are depicted in figures 13–15 for the heating rate of $Q \sim 3Q_c = 700$ W. Figures 13(*a*) and 13(*b*) depict, respectively, $\Delta T_{3-9}$ and $\Delta T_{6-12}$ as functions of time. The motion appears to

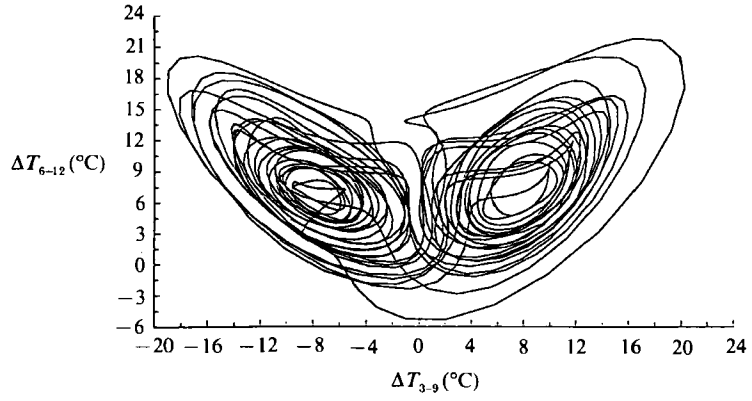


FIGURE 14. The experimentally measured temperature difference $\Delta T_{3-9}$ is depicted as a function of the temperature difference $\Delta T_{6-12}$ for the uncontrolled system. $Q = 700$ W.

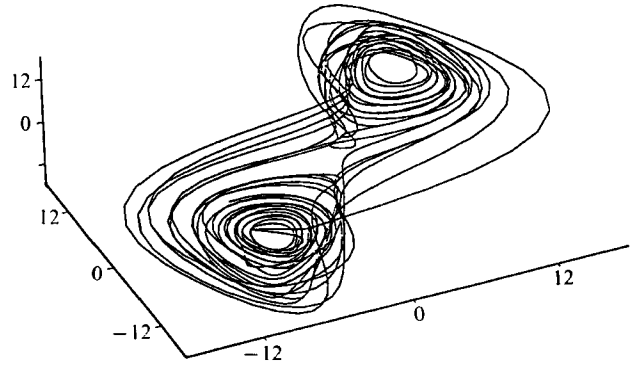


FIGURE 15. The attractor is reconstructed, using the time delay technique (with a time delay of 10 s), in a three-dimensional embedding space from the time series depicted in figure 13(*a*). $Q = 700$ W.

consist of irregular oscillations in the flow rate. Positive and negative $\Delta T_{3-9}$ correspond to counterclockwise ($u > 0$) and clockwise ($u < 0$) motions, respectively. Witness the relatively high temperature oscillations associated with the non-steady flow. The experimental time series (figure 13*a*) qualitatively resembles the time series depicted in figure 3, which was obtained from the mathematical model. Similar flows were observed by Creveling *et al.* (1975) and Gorman *et al.* (1984, 1986). Since the largest Lyapunov exponent associated with this flow is positive (Singer 1991), we conclude that the flow is chaotic.

In figure 14, we depict $\Delta T_{3-9}$ versus $\Delta T_{6-12}$ to obtain a phase portrait of the system while in figure 15, we show a three-dimensional portrait of the attractor constructed from the $\Delta T_{3-9}$ time series (figure 13*a*) using the time delay technique and a three-dimensional embedding space. The correlation dimension of the attractor is estimated as $\sim 2.2$ (Singer 1991). The experimental phase-space portraits in figures 14 and 15 resemble the now well-known phase portraits of the Lorenz (1963) attractor which were obtained from numerical integrations of (6)–(8).

Interesting though the chaotic motion might be, the study of its dynamics is not the subject of this paper. The description above was presented for two reasons: first, to acquaint the reader with the phenomena observed in the loop in the absence of a control mechanism; and second, to demonstrate that the mathematical model

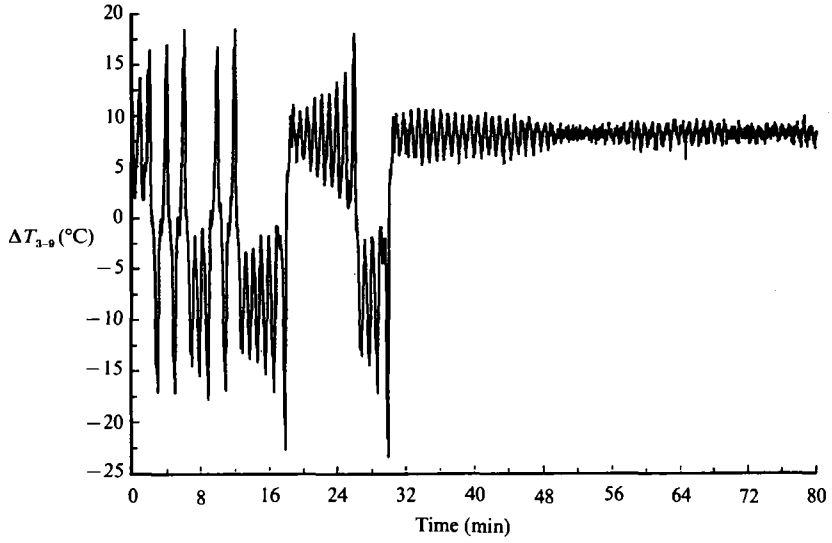


FIGURE 16. The experimentally measured temperature difference $\Delta T_{3-9}$ is depicted as a function of time for a heating input of 700 W. The controller was activated 33 minutes into the run.

presented in §2 is capable of providing a qualitative description of the flow phenomena observed in the loop.

### 3.3. *The controlled system*

The theoretical investigation presented in §2 suggests that the characteristics of the motion can be modified considerably with the use of a controller. In this section, we wish to demonstrate that these ideas can be used in practice. For example, suppose the chaotic oscillations observed in figures 13–15 are an undesired phenomenon. We wish to suppress this oscillatory behaviour and make the flow approximately steady while operating at power levels which nominally yield chaotic motion. Our goal is to achieve this objective without affecting the system's structure and with minimal changes in the power input.

To accomplish this objective, we adopt the proportional control strategy described in §2.3. For the steady, non-chaotic motion, the temperature difference is time-independent. We denote this time-independent value as $\overline{\Delta T_{3-9}}$. Next we argue that the steady solution, albeit non-stable, still exists in the chaotic regime for $Q = Q_0 > Q_c$, where $\Delta T_{3-9}$ is now time-dependent. We wish to modify the heat input to the loop in proportion to the deviations of $\Delta T_{3-9}$ from the desired value $\overline{\Delta T_{3-9}}$. To this end, we set the feedback $Q = Q_0 + K(\Delta T_{3-9} - \overline{\Delta T_{3-9}})$. The $\overline{\Delta T_{3-9}}$ value which corresponds to $Q_0$ need not be accurately known. If, for example, we err in estimating the correct value of $\overline{\Delta T_{3-9}}$, the controller will adjust the average power level so that $\overline{\Delta T_{3-9}}$ corresponds to the time-independent state.

The results of this strategy are depicted in figure 16 where we show the temperature difference between the 3 and 9 o'clock positions depicted as a function of time for a nominal heat input $Q_0 \sim 3Q_c = 700$ W. To contrast the uncontrolled and controlled behaviour, we depict initially ($t < 33$ minutes) the uncontrolled flow in figure 16. Note the oscillatory behaviour similar to that depicted in figures 3 and 13. The controller with a gain of $K = -39$ W/°C, was activated 33 minutes into the run. The transition from the chaotic flow into a relatively steady, laminar flow is self-evident. We ran the experiment for over 15 hours, maintaining the type of steady flow

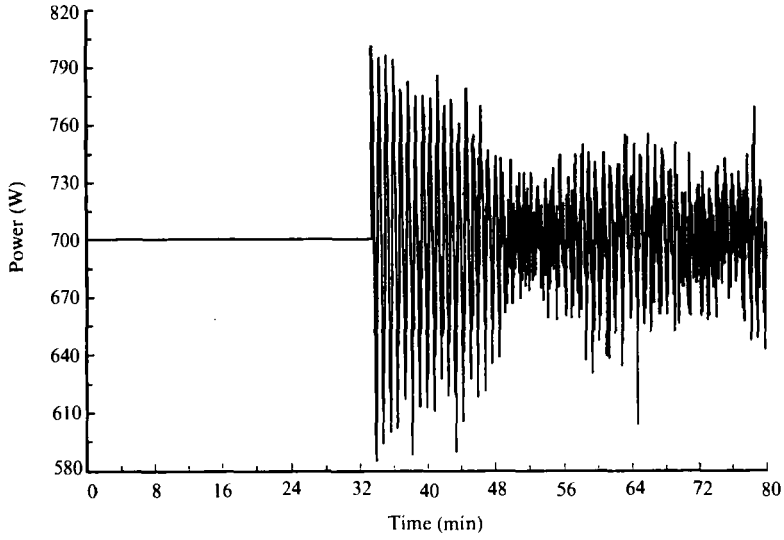


FIGURE 17. The power variations mandated by the controller are depicted as functions of time. The controller was activated 33 minutes into the run.

shown in figure 16 for $t > 60$ minutes. The controller also succeeded in overcoming finite-amplitude disturbances deliberately introduced into the loop. The power variations mandated by the controller are depicted in figure 17. Once the flow has been brought close to its steady-state value, the power variations required to maintain this value are within $(1 \pm 0.08) Q_0$.

Next, we investigated the minimal gain required to maintain the steady flow in the chaotic regime. This was done by stabilizing the flow with a relatively large negative gain and then gradually decreasing the absolute magnitude of the gain until oscillatory behaviour was observed. We found this minimal gain to be approximately $K = -27$ W/°C; and within the experimental precision, it appears to be independent of the nominal heat input $Q_0$. This is in contrast to the predictions of the mathematical model which suggested that the marginal value of $K$ would decrease as the heating rate (or the Rayleigh number) increased. This deviation can be attributed to the fact that the mathematical model we used is too simple to provide accurate quantitative predictions. Also, the Prandtl number ($P$) in the experiment is not a constant, declining as the power input is increased. In contrast, the mathematical model assumes $P$ is constant.

To illustrate how the controller operates, we briefly describe the mechanism responsible for the chaotic, oscillatory behaviour of the flow in the loop (Welander 1967). To this end, imagine that a small disturbance causes the flow to slow down below the steady-state flow rate. As a result, the fluid spends more time in the heater/cooler section, gains/loses more/less heat than usual and emerges from the heater/cooler with a temperature higher/lower than usual. This, in turn, causes an increase in the buoyancy force with a corresponding increase in the fluid velocity. Once the fluid velocity increases, the process reverses itself. Under appropriate conditions, these oscillations amplify and, in the uncontrolled system, eventually lead to the chaotic behaviour depicted in figures 13–15. In contrast, when the controller is operating, it detects the appearance of disturbances by monitoring deviations in the temperature difference $\Delta T_{3\text{-}9} - \overline{\Delta T_{3\text{-}9}}$. Once a deviation is detected, the controller takes action to counteract its effect. For instance, if the deviation

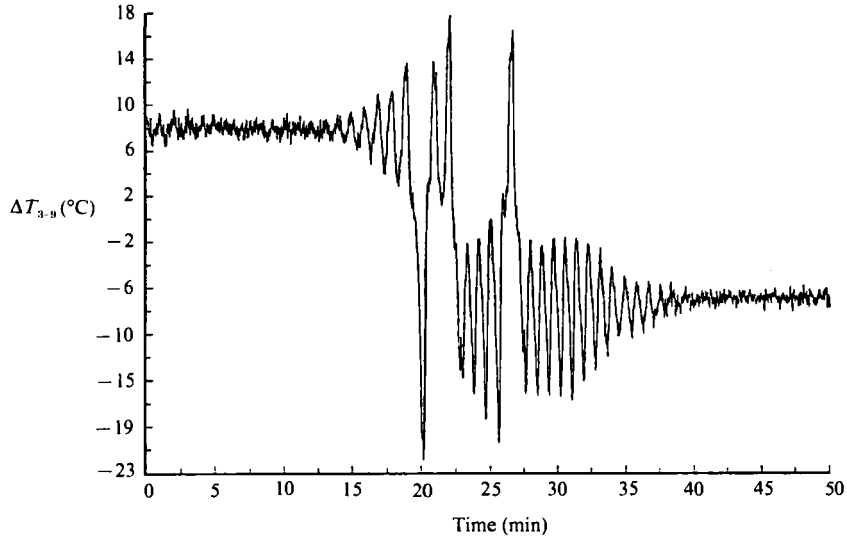


FIGURE 18. The controller is being used as a device for switching the direction of the flow ($Q = 700$ W). For $t < 12.5$ ($K = -78$ W/°C) and $t > 12.5$ ($K = 78$ W/°C), the controller stabilizes the counterclockwise and clockwise motions, respectively.

tends to accelerate/decelerate the flow, the heating rate is increased/decreased to counteract this effect. As the controller applies only relatively small perturbations to the input power, it will be able to counteract only small oscillations. Consequently, if one wishes to control an already chaotic flow, one may need to wait to activate the controller until the system comes into the vicinity of the state we wish to maintain. The size of the basin of attraction of the controlled flow typically increases with increasing absolute gain. Once the controller succeeds in laminarizing the flow, it will prevent the oscillations from increasing beyond the controllable magnitude.

We note in passing that, with the aid of the controller, we could have brought the system up to a desired power level without ever observing chaotic behaviour. This, of course, may be the desired mode of operation in practical applications. However, for illustration purposes, we demonstrated here that the controller can successfully perform the more daunting task of suppressing the chaotic behaviour once it has already occurred. It also should be noted that we made no attempt to optimize the controller and that it is likely that the magnitude of the control signal can be reduced further by adopting a more sophisticated control strategy than the one reported here.

Since the controller can stabilize either the counterclockwise or the clockwise motion, it can be used as a switch effecting a change in the flow direction. This is demonstrated in figure 18 where we initially stabilized the flow in the counterclockwise direction ($Q = 700$ W, $K = -78$ W/°C). At time $\sim 12.5$ minutes, we changed the control strategy so as to stabilize the clockwise motion by flipping the sign of $K$ (i.e. $K = 78$ W/°C). As a result, we managed to reverse the direction of the flow at will.

Finally, we demonstrate that the controller can be used to induce chaos under circumstances in which chaos will not normally occur. To this end, we use a positive feedback and adopt a similar control strategy to the one used in the mathematical model, i.e. $Q = Q_0 + K[\mathrm{sgn}(\Delta T_{3-9})\Delta T_{3-9} - \overline{\Delta T_{3-9}}]$. The results of this strategy are depicted in figure 19, where we show the temperature differences $\Delta T_{6-12}$ and $\Delta T_{3-9}$ as

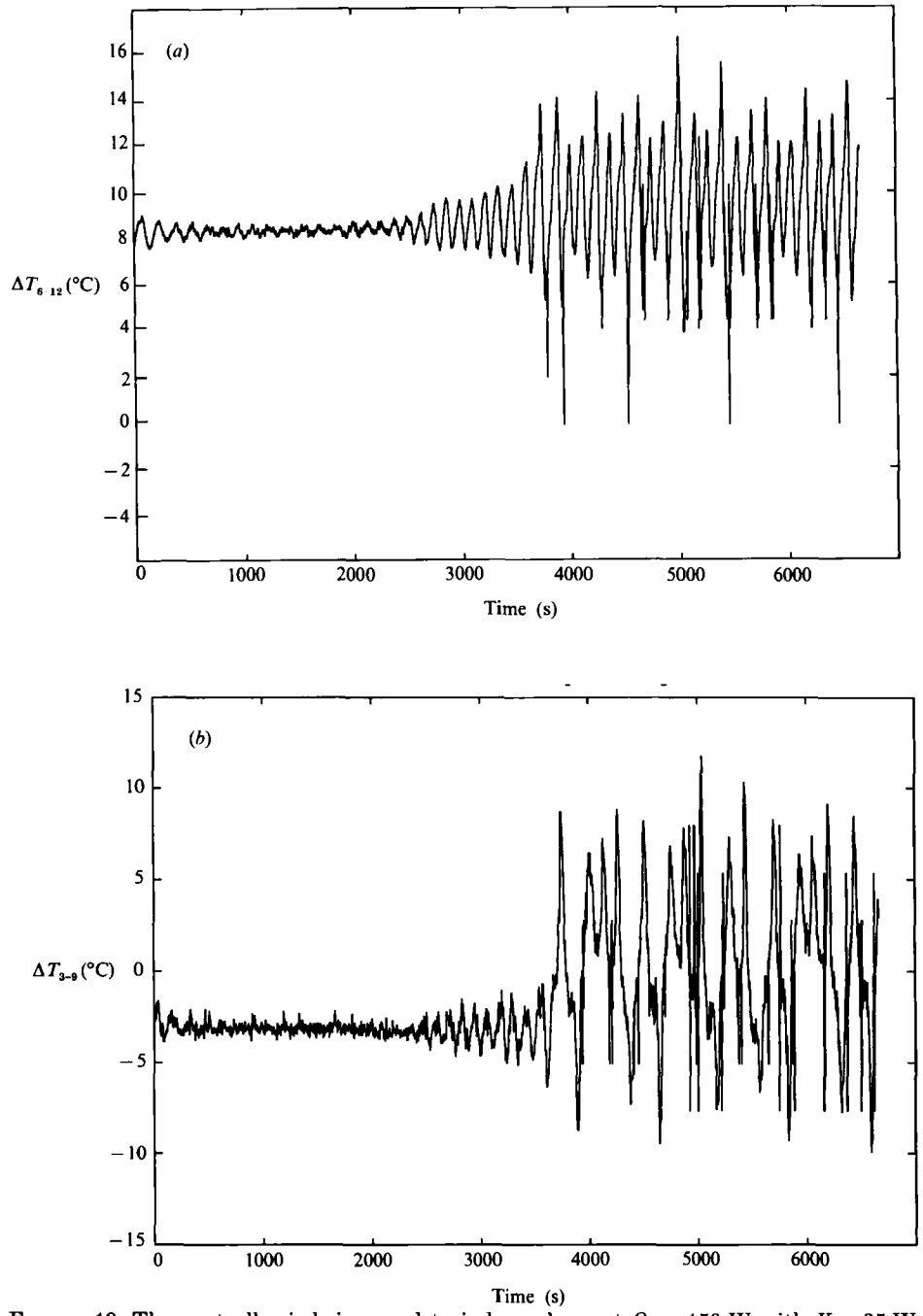


FIGURE 19. The controller is being used to induce chaos at $Q_0 = 150$ W with $K = 35$ W/°C. The uncontrolled system will not exhibit chaotic behaviour until $Q \sim 250$ W. The figure depicts the temperature difference (*a*) between the 3 and 9 o'clock positions and (*b*) between the 6 and 12 o'clock positions as functions of time.

functions of time for the nominal power input $Q = 150\ W \sim 0.6Q_c$. In the absence of a controller, the transition to chaos occurs at about $Q_c \sim 250$ W. To illustrate the difference between the uncontrolled and controlled systems, we depict initially the uncontrolled behaviour for $t < 1800$ s. Witness the relatively time-independent, counterclockwise motion. The controller, with a gain $K = 39$ W/°C, was activated at $t = 1800$ s. It causes flow instabilities to amplify, as is evident in figure 19, until eventually chaotic flow develops. Owing to the relatively large-amplitude oscillations of $\Delta T_{3\text{-}9}$, the control strategy requires power variations over a fairly substantial interval. The average power supplied to the loop in the chaotic regime was about 170 W, somewhat higher than the nominal power $Q_0$. We succeeded in destabilizing time-independent flows and obtaining chaotic behaviour at heating rates as low as 100 W.

## 4. Conclusion

The use of active (feedback) control to modify various physical processes such as noise and vibrations has attracted a considerable amount of interest. Surprisingly, not withstanding the plethora of potential applications, very little has been done in using active control to modify convective processes. In this paper, we have demonstrated both theoretically and experimentally that active control can be used to significantly alter the flow characteristics of a simple convective system. Whether these or similar ideas also can be implemented in more complicated situations, such as those involving Bénard convection, is still an open question; but it is certainly one worth pursuing.

This work was supported, in part, by the National Science Foundation through Grant CBT 83-51658. Mr Kevin Turk assisted us with some of the experiments.

## REFERENCES

Bau, H. H. & Torrance, K. E. 1981 Transient and steady behaviour of an open symmetrically-heated, free convection loop. *Intl J. Heat Mass Transfer* **24**, 597–609.

Bau, H. H. & Wang, Y.-Z. 1991 Chaos: a heat transfer Perspective. In *Annual Reviews in Heat Transfer*, Vol. IV (ed. C. L. Tien), pp. 1–50. Hemisphere.

Creveling, H. F., De Paz, J. F., Baladi, J. Y. & Schoenhals, R. J. 1975 Stability characteristics of a single phase thermal convection loop. *J. Fluid Mech.* **67**, 65–84.

Ditto, W. L., Rauseo, S. N. & Spano, M. L. 1990 Experimental control of chaos. *Phys. Rev. Lett.* **65**, 3211–3214.

Ehrhard, P. & Muller, U. 1990 Dynamical behaviour of natural convection in a single-phase loop. *J. Fluid Mech.* **217**, 487–518.

Gorman, M., Widmann, P. J. & Robins, K. A. 1984 Chaotic flow regimes in a convection loop. *Phys. Rev. Lett.* **52**, 2241–2244.

Gorman, M., Widmann, P. J. & Robins, K. A. 1986 Nonlinear dynamics of a convection loop: a quantitative comparison of experiment with theory. *Physica* **19D**, 255–267.

Hart, J. E. 1984 A new analysis of the closed loop thermosyphon. *Intl J. Heat Mass Transfer* **27**, 125–136.

Hart, J. E. 1985 A note on the loop thermosyphon with mixed boundary conditions, *Intl J. Heat Mass Transfer* **28**, 939–947.

Iooss, G. & Joseph, D. D. 1989 *Elementary Stability and Bifurcation Theory*, 2nd edn. Springer.

Lorenz, E. N. 1963 Deterministic nonperiodic flow. *J. Atmos. Sci.* **20**, 131–141.

Malkus, W. V. R. 1972 Non-periodic convection at high and low Prandtl number. *Mem. Soc. R. Sci. Liege* **IV** (6), 125–128.

METROL, A. & GREIF, R. 1985 A review of natural circulation loops. In *Natural Convection: Fundamentals and Applications* (ed. W. Aung, S. Kakac & R. Viskanta), pp. 1033–1081. Hemisphere.

OTT, E., GREBOGI, C. & YORKE, J. A. 1990*a* Controlling chaos. *Phys. Rev. Lett.* **64**, 1196–1199.

OTT, E., GREBOGI, C. & YORKE, J. A. 1990*b* Controlling chaotic dynamical systems. In *Chaos: Soviet–American Perspectives on Non-linear Science* (ed. D. K. Campbell), pp. 153–172. Am. Inst. Phys.

OTTINO, J. M 1989 *The Kinematics of Mixing: Stretching, Chaos and Transport.* Cambridge University Press.

SINGER, J 1991 Controlling a chaotic system. MS thesis, University of Pennsylvania.

SINGER, J. & BAU, H. H. 1991 Active control of convection. *Phys. Fluids* A (to appear).

SINGER, J., WANG, Y.-Z. & BAU, H. H. 1991 Controlling a chaotic system, *Phys. Rev. Lett.* **66**, 1123–1126.

SPARROW, C. 1982 *The Lorenz Equations: Bifurcations, Chaos, and Strange Attractors.* Springer.

WANG, Y.-Z. 1991 Problems in thermal convection. Ph.D. thesis, University of Pennsylvania.

WANG, Y.-Z. & BAU, H. H. 1990 Period doubling and chaos in a thermal convection loop with time periodic wall temperature variation. *Intl Heat Transfer Conf.* 90, Vol. II, pp. 357–362.

WANG, Y.-Z. & BAU, H. H. 1991 Thermal convection loop with heating from above. *Int J. Heat Mass Transfer* (to appear).

WELANDER, P. 1967 On oscillatory instability of differentially heated fluid loop. *J. Fluid Mech.* **29**, 17–30.

WIDMANN, P. J., GORMAN, M. & ROBINS, K. A. 1989 Nonlinear dynamics of a convection loop II: chaos in laminar and turbulent flows. *Physica D* **36**, 157–166.

YORKE, A., YORKE, E. D. & MALLET-PARET, J. 1987 Lorenz-like chaos in partial differential equation. *Physica* **24D**, 279–291.